SOFTWARE SIMULATION OF THE TONE-HOLE LATTICE IN CLARINET-LIKE SYSTEMS

Fritz Schueller, Carl Poldy

Private Researchers
Vienna, Austria

fritz.schueller@aon.at
carl.poldy@nativeprogramming.at

ABSTRACT

Arthur Benade introduced the notion of a tone-hole lattice in the early 1960s. He found that there exists a so-called "cutoff frequency" that is determined by the structural dimensions of the tube and its side-holes. Since then several other researchers have studied the properties of the tone-hole lattice, especially dealing with the row of open tone-holes. When simulating mechanical and acoustical systems it is convenient to use electromechanical and electro-acoustical analogies. Highly developed theories for electric networks can thus be directly used to simulate the behaviour of musical instruments.
Special software applications, such as Micro-CAP by Spectrum Software of California, an electrical Circuit Analysis Program, can be used for this purpose. To build a bridge from the electrical to the mechanical and acoustical world there exist so called "macros" that were developed mainly by the second author, with mechanical input parameters, so the user need not necessarily think in electrical terms. Examples of such macros are two-ports representing lossy cylindrical and conical tubes, two-poles for short holes etc. all of which occur in wind instruments. Other useful two-ports are ideal transformers for coupling mechanical and acoustical parts of the model.
The impedance-versus-frequency diagrams that are easily derived with the aid of Micro-CAP can help to detect influences of the several dimensions of the tone hole system. It is also possible to show pressure and flow profiles along the axis of the tube with opened and closed side-holes. Such work can lead to a further understanding of the properties of real woodwind instruments.

1. INTRODUCTION

The applicability of the simulation tool for the tone-hole lattice was tested using the work of Benade as an entry point. In his book Fundamentals of Musical Acoustics [2], Benade gives an example of a tube 61 cm long extended by a tube with side holes. The impedance curve is shown in Fig. 21.3 of the book. No more details about the tube are given there. Using the simulation tool, the authors were able to reconstruct approximately the dimensions of the tube Benade used for his measurement. The influence of the cutoff frequency can be seen clearly.

Throughout this article geometrical parameters are used with the symbols Benade introduced in [1]. The diameter of the cylindrical bore is *2a*, the radius of a tone hole is *2b* and the distance between the holes is *2s*. For the depth of the hole (thickness of the wall) the symbol *t* is used.

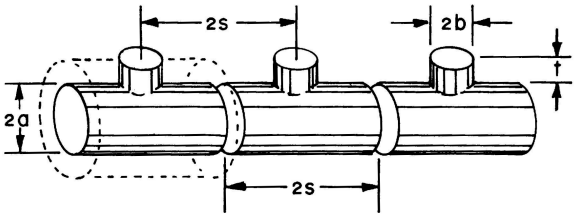

Fig. 1, Arthur H. Benade's tone-hole lattice

Three T-shaped elements of the tone-hole lattice are shown in Fig.1 (copy of the upper part of Fig. 21.8 on page 448 of [2]). Here we deal only with the lattice of open tone holes. Thus the air in the holes can move freely and an inner and outer end-correction needs to be taken into account. Benade uses the definition $t_e = t+1.5b$ for the effective length of the side holes.

Section 2 is an attempt to reconstruct the tone-hole lattice that Benade measured to get Fig. 21.3 (page 435 of [2]). In section 3 the impedance curves for the non-lossy case, based on an article of Moers and Kergomard [4] are shown. And finally section 4 shows a simulation of the lossy case, using the macro for lossy tubes with circular cross section.

The main purpose of the present article is to check the simulation against the measurement results and theoretical formulations. The whole article is about the regular tone-hole lattice. But different values of *a, b, s,* and t_e are used in the three following sections. For all simulations the speed of sound is taken to be 346.2 m/s, the viscosity coefficient 1.86×10^{-5} kg/(ms) and the density 1.186 kg/m^3 (air at *23°C*).

2. BENADE'S TONE-HOLE LATTICE

Beginning on page 434 of [2] Benade gives an incomplete description of the geometrical setup for the curves of Fig. 21.3 [2]. For the upper curve (pipe alone) he quotes a length of 61 cm and a first peak of the input impedance at 140 Hz.

The simulation in Fig. 2 corresponds to the lower half of Fig. 21.3 [2]. The dimensions are given in the figure directly. The first part of Benade's tube (containing no holes) had to be shortened to 542 mm to keep the first resonance at 140 Hz.

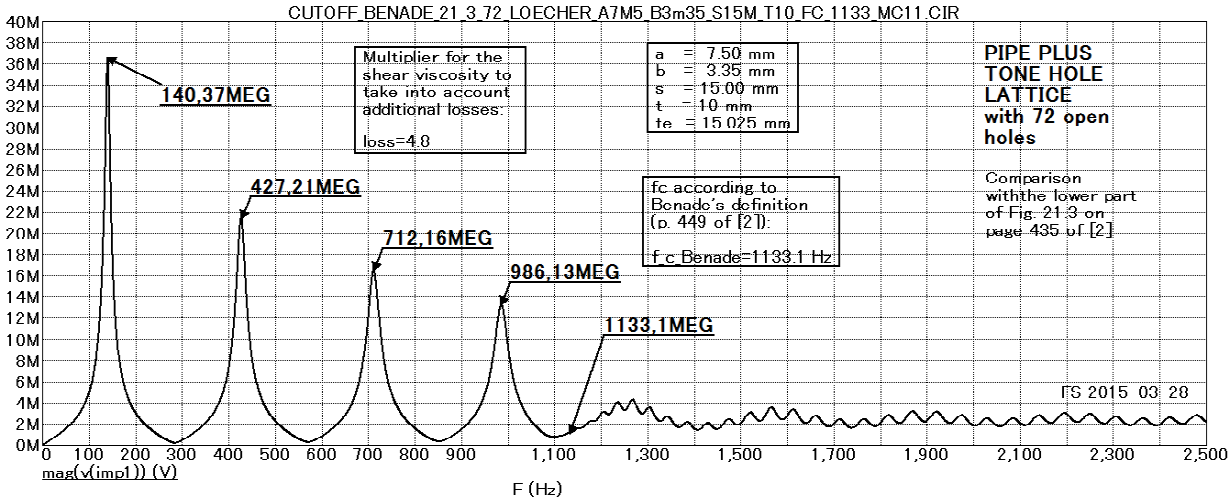

Fig. 2, Reconstruction of Benade's experiment

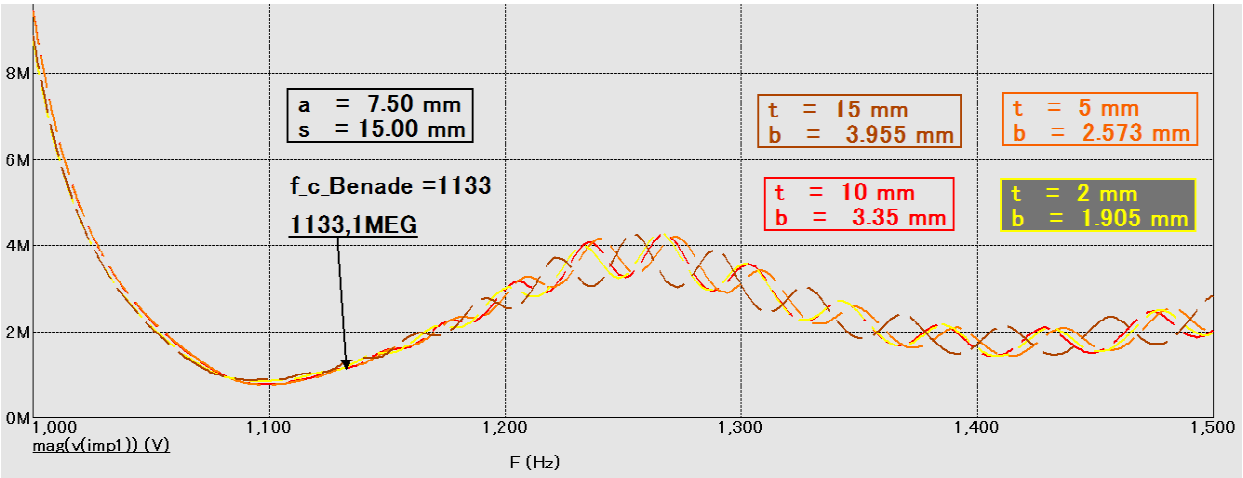

Fig. 3, f_c constant, *t* and *b* variable

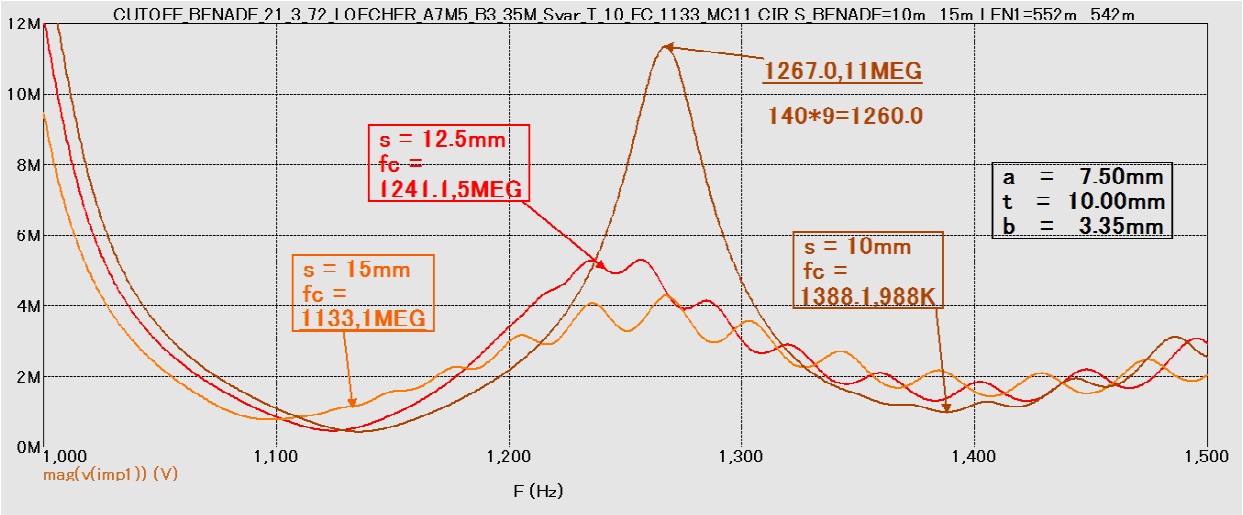

Fig. 4, *s* variable, leading to different values of f_c

The simulation is based on an increased value for the shear viscosity ($4.8 \times 1.86 \times 10^{-5}$ kg/m/s). The factor 4.8 was found experimentally, in order to achieve a similar height of the impedance peak at 140 Hz as Benade measured. A minimal number of 72 open holes is needed to bring the peaks to the right of the cutoff frequency down to less than 4 MOhm (corresponding to Fig. 21.3 of [2]). It is important to stress that the cutoff frequency as indicated in the figure is calculated for the non-lossy case, as stated in [1] in the text (damping is neglected) above equ. (8). The simulation however - as in Benade's experiment - involves lossy tube- and lossy hole-elements.

Some interesting experiments can now be done with the model. Using the same sizes for *a* and *s* as before, but changing *b* and *t* in such a way that f_c stays at 1133 Hz, one obtains the result of Fig. 3. Here the *x*- and *y*-ranges have been reduced compared to Fig. 2. We see here that there is not much difference in the overall picture. Only the peaks of the wiggling part above cutoff occur at different frequencies. The envelope curve does not change at all.

In the next experiment all geometrical parameters except *s* are kept constant. This leads to different cutoff frequencies, as can be seen in Fig. 4. For the smallest *s* (10 mm) the fifth resonance peak of that part of the tube without holes (approx. 9 times 140 Hz) falls below cutoff, thus not affecting the peak very much. The tube without holes had to be lengthened for the smaller values of *s*, to keep the basic resonance at 140 Hz (552mm for *s*=10mm, 547mm for *s*=12.5mm).

3. TWO TREATMENTS OF THE NON-LOSSY CASE

Benade gives a formula for f_c in [2] on page 449:

$$f_c = 0.110\ (b/a)\ c\ [1/(s\,t_e)]^{1/2} \qquad (1)$$

This formula was used for calculating f_c in the preceding section although it contains a small rounding error. Setting the denominator to zero in the original formula (8) of [1] gives the correctly rounded value of *0.109* as the first factor. In this section the more accurate value is used to calculate Benade's cutoff frequency.

The original formula (8) of [1] is shown here (2):

$$Z_0 = \left(\frac{\rho\, c}{\pi a^2}\right)\left(\frac{1+\frac{1}{2}(b/a)^2\, cot(\omega t_e/c)\, tan(\omega s/c)}{1-\frac{1}{2}(b/a)^2\, cot(\omega t_e/c)\, cot(\omega s/c)}\right)^{1/2} \qquad (2)$$

Solving for zero in the denominator was done with MicroCAP by searching the pole of the reciprocal value of the denominator on the frequency scale. Since the circuit analysis program has numerical limitations a very big but finite value is the result for the peak height.

Using the parameters of Fig. 2, the cutoff frequency now becomes 1123 Hz (=1133 x 0.109/0.110).

But there is also another value of the cutoff frequency, that can be derived from the article of Moers and Kergomard [4]. On page 986 of [4] we see the elements of the transfer matrix of a single T-shaped element for the non-lossy case. Z_c (corresponding to Benade's Z_o, "o" probably standing for "open") is not given explicitly in [4]. But it can be easily calculated by substituting the matrix elements *B* and *C* into the equation for Y_c^2 (given below equation (2) on page 986).

By eliminating all the abbreviations used in *B* and *C* and using Benade's symbols one obtains for Z_c:

$$Z_c = \left(\frac{\rho\, c}{\pi a^2}\right)\left(\frac{1+\frac{1}{2}(b/a)^2\, (c/(\omega t_e))\, tan(\omega s/c)}{1-\frac{1}{2}(b/a)^2\, (c/(\omega t_e))\, cot(\omega s/c)}\right)^{1/2} \qquad (3)$$

A detailed derivation and a comparison with equation (8) of [1] can be found in the appendix 1.

Moers and Kergomard [4] give a good approximation of f_c in (6) on page 987. It is very close to the frequency where the denominator of Z_c becomes zero. Rounded to one Hz f_c is 1140Hz in both cases, either using (6) or looking for the pole of Z_c calculated from the matrix elements *B* and *C*.

Next we see a simulation using a number of simple T-shaped elements (100 elements all in one dimension). Fig. 5 shows the beginning of the tone-hole lattice. Included are the impedance sensor at the input and one of the T-shaped elements. Grounding means that an aperture is open because a current (volume flow) can flow into zero voltage (zero pressure).

The two components of the T-shaped element are a non-lossy tube (transmission line) and a non-lossy inductor. The tube elements are simply delay lines, giving a delay corresponding to the speed of sound *c* and the length *s* of the element. The inductor represents the acoustic mass of the air in the hole (including inner and outer end-corrections). The inductance becomes $L = \rho t_e/(\pi b^2)$, taking into account that the acoustic part is linked to the electrical part by a factor of $1/area^2$ $(area=\pi b^2)$. The density of air at *23°C* is $\rho = 1.186 kg/m^2$ in these simulations.

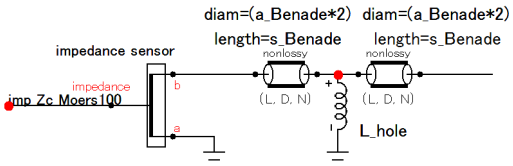

Fig. 5, Impedance sensor and one T-shaped element

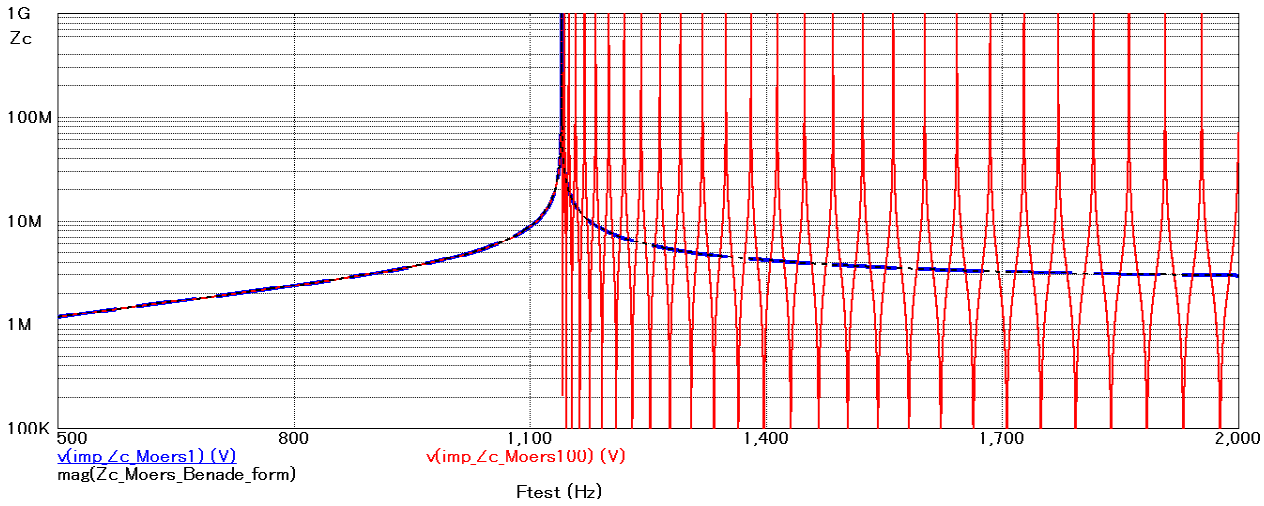

Fig. 6, Input impedance of tone-hole lattice with 100 open holes and Z_c

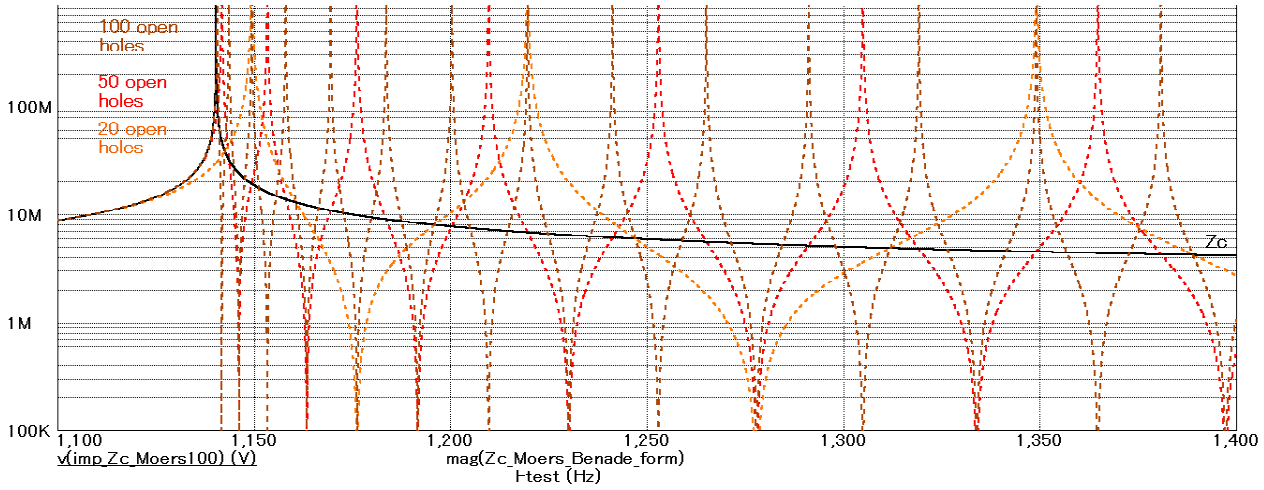

Fig. 7, Input impedance of tone-hole lattices with, 100, 50 and 20 open holes and Z_c

Now the simulation is used to show the agreement of the formula for Z_c with the model. The magnitude of the input impedance for a tone-hole lattice with one hundred open holes is shown (Fig. 6). Unlike the preceding section, there is no part of the tube without side holes. As there are no losses, the peaks theoretically go to infinity and the minima are zero. It is interesting to see that the peaks come closer together, when approaching f_c from higher frequencies. Reducing the number of open holes leads to fewer peaks and fewer minima and the lowest peak moves further away from f_c. Fig. 7 shows the situation for 100, 50 and 20 open holes in a smaller frequency range than before (again no damping). Fig. 7 shows the same for 100, 50 and 20 open holes in a smaller frequency range than before (again no damping).

4. PRESSURE AND FLOW ALONG THE TUBE, LOSSY CASE

We return now to the model with losses. Again there is an artificial increase of the shear viscosity used, as described in section 2 (4.8 x 1.86 x 10^{-5} kg/m/s). The T-shaped element now consists of tube elements (macros) only (see Fig. 8). A detailed description of the tube model is given in appendix 2. The tube elements themselves do not contain any end correction. Therefore the length of the side hole (tube) has to be set to t_e (Benade's fomula $t_e = t + 1.5b$ is used). The measuring points *Px* and *Fx* will be described later in this section. There are 68 open side holes used in the following experiments. At the end of the complete lattice a radiator is placed, as shown in Fig. 9.

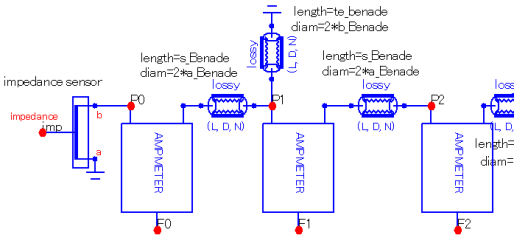

Fig. 8, Setup for impedance measurement; impedance sensor, ampere meter, measuring points

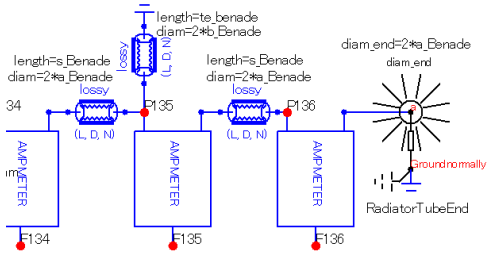

Fig . 9, End of the tone-hole lattice, with radiator

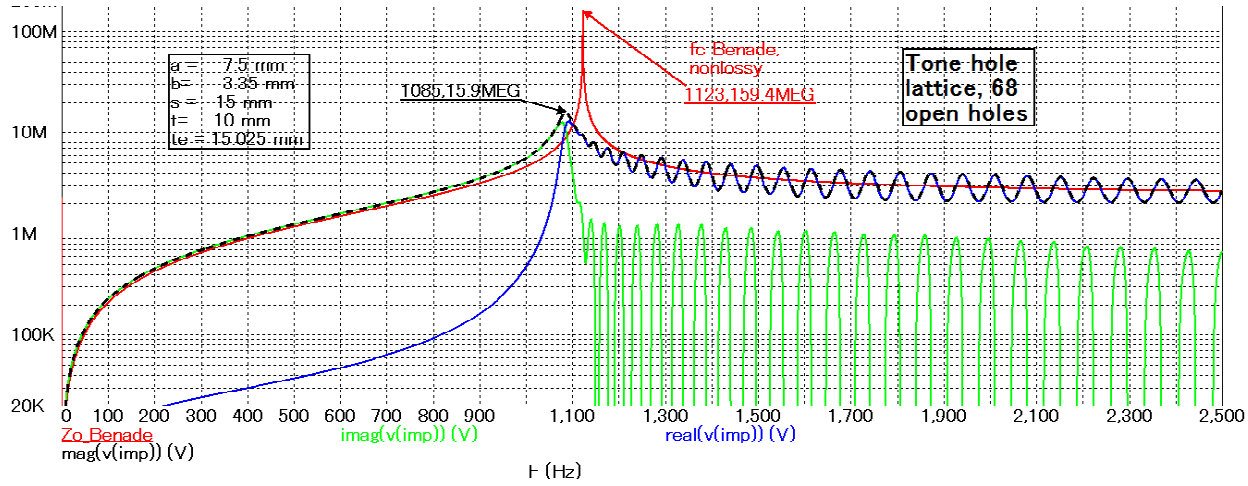

Fig. 10, impedance chart for 68 open holes

The input impedance is computed and shown in Fig. 10. As there are losses, according to the theory there is also a small real part below cutoff (blue) and a small imaginary part above cutoff (green). Benade's f_c (non-lossy case) is indicated for comparison (red). There are more resonances in the range above 5 kHz, also including a negative imaginary part. This is not considered further here.

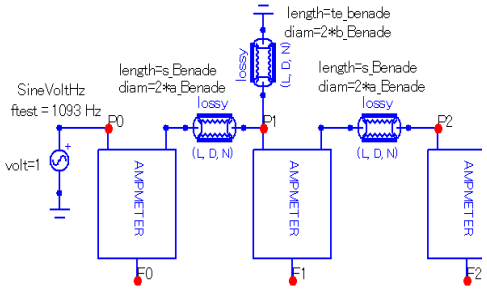

Fig. 11, Setup for pressure and flow measurement

Now to get an idea of the pressure and flow in the tube, the impedance sensor is replaced by a sine voltage source (Fig. 11). The frequency of the peak (1093 Hz) is chosen for the experiment and the voltage is set to 1V (1Pa). The result (Fig. 12 and Fig. 13) is not a simple standing wave, but a combination of a standing wave and a travelling wave. For a pure standing wave, the imaginary part of the pressure would be zero along the whole tube.

Voltages at points *Px* (x=0 ... 136) correspond to pressure values (Pa), voltages at points *Fx* (x=0 ... 136) to volume flow (m^3/s). Point *P0* (*F0*) would be the mouthpiece tip of a woodwind instrument, *P136* (*F136*) the end of the bell. The open holes are at the positions *Px* with x being an odd number (1 to 135).

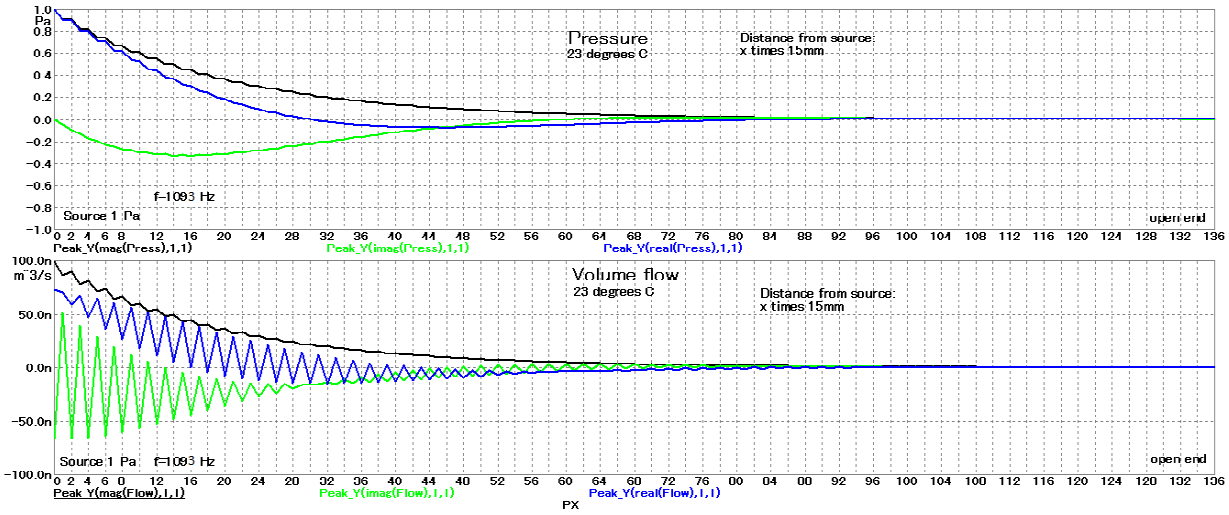

Fig. 12, Pressure and volume flow along the tube with 68 open holes

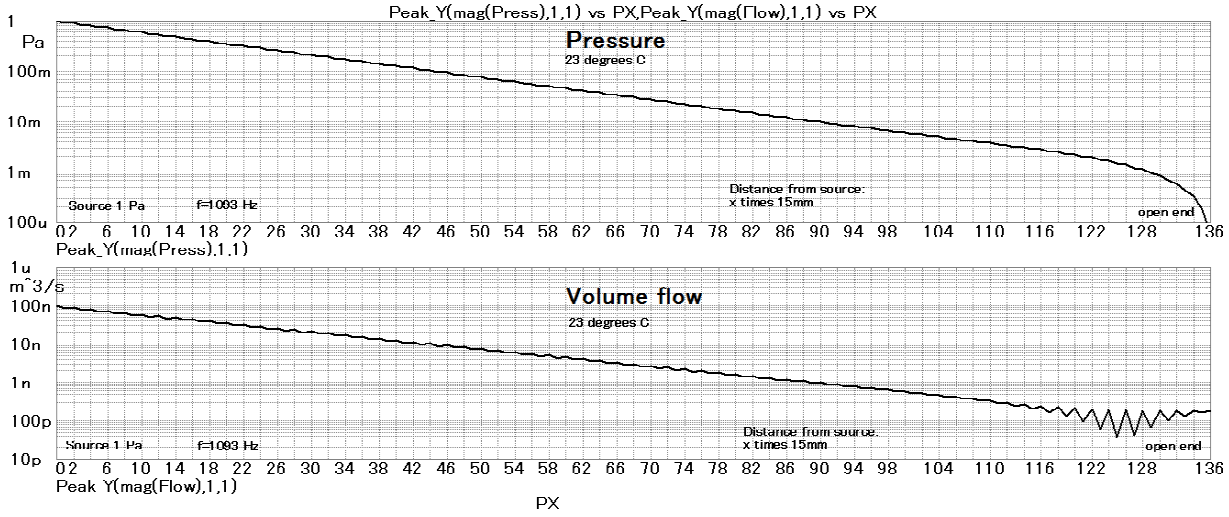

Fig. 13, Magnitude of pressure and flow along the tube with 68 open side holes, logarithmic scale

5. CONCLUSION

In this article some simple structures of tone-hole lattices were analysed showing the suitability of an electronic circuit analysis program to study acoustical questions concerning musical wind instruments. It can be seen that there is good agreement with theory and experiments in the relevant literature. This opens the way to study many other questions. This could be the impedance, pressure and flow properties of wind instruments with irregularly placed tone-holes (which is the normal case). There also exist macros for conical tubes, tubes with rectangular cross section, etc., developed by the second author. Thus also conical instruments, such as oboes, bassoons and saxophones could be studied.

The user interface and the circuit diagrams are very intuitive, so the use of this kind of software simulation is also valuable for teaching and studying. There exists more literature treating the cutoff frequency and the side hole, e.g. [5], [6], [7] and [8] that could be used for a cross check. But most important is the fact that real instruments could be analysed, based on the geometrical dimensions of the bore and the holes.

The method of raising the shear viscosity to cope for losses that are not known in detail could be improved by looking into the cause of the losses (turbulence, porosity, friction, radiation, etc.) and trying to model these parameters effectively.

A very ambitious aim would be to try to include nonlinear effects and/or two-dimensional simulations. This would mean developing new, probably rather complicated macros.

6. APPENDIX 1

Here it is described how to express the characteristic impedance Z_c from Moers and Kergomard [4] in a form similar to that which Benade used in [1].

First the matrix elements *B* and *C* [4] are divided by j. Then the variables *Y*, Z_c, *k* are replaced by ω *(=2πf)*, ρ (density of air), *c* (speed of sound), *a* (tube radius), *b* (hole radius) and t_e (effective hole depth). For the length of the tube elements *s* is used, as Benade did in [1]. All necessary formulae for these replacements can be found on page 986 and 987 of [4].

This gives *B/j* and *C/j* in the form of

$$B/j = \frac{\rho c}{\pi a^2}\left[2\,sin\,(\omega s/c)\;cos\,(\omega s/c) + (b/a)^2\;(c/(\omega t_e))\,cos^2\,(\omega s/c)\right] \quad (4)$$

$$C/j = \frac{\pi a^2}{\rho c}\left[2\,sin\,(\omega s/c)\;cos\,(\omega s/c) - (b/a)^2\;(c/(\omega t_e))\,cos^2\,(\omega s/c)\right] \quad (5)$$

Therefore *Zc =1/Yc* becomes

$$Z_c = \sqrt{\frac{B}{C}} = \frac{\rho c}{\pi a^2}\left[\frac{2\,sin\,(\omega s/c)\;cos\,(\omega s/c) + (b/a)^2\;(c/(\omega t_e))\,cos^2\,(\omega s/c)}{2\,sin\,(\omega s/c)\;cos\,(\omega s/c) - (b/a)^2\;(c/(\omega t_e))\,cos^2\,(\omega s/c)}\right] \quad (6)$$

Now reducing the fraction by

$$2\,sin\,(\omega s/c)\;cos\,(\omega s/c) \quad (7)$$

gives Z_c in a similar form as the Z_o in (8) of [1].

$$Z_c = \left(\frac{\rho c}{\pi a^2}\right)\left(\frac{1 + \frac{1}{2}(b/a)^2\,(c/(\omega t_e))\,tan(\omega s/c)}{1 - \frac{1}{2}(b/a)^2\,(c/(\omega t_e))\,cot(\omega s/c)}\right)^{1/2} \quad (8)$$

Comparing the two equations for Z_c and Z_o (8), one finds that only the term *cot(ωt$_e$/c)* in (8) is replaced by *c/(ωt$_e$)*.

Remark: Benade uses Z_c for "*Z* for tubes with *closed* holes" and Z_o for "*Z* for tubes with *open* holes", whereas in [4] Z_c stands for "characteristic impedance".

These two functions are very similar for frequencies where *λ/4* is much bigger than t_e. This is valid for the cutoff frequency of 1140 Hz and t_e being about *15mm*. Benade evidently treated the side-hole as a tube, whereas Moers simplified the model to a rigid mass in the side hole. The latter method is sufficient for many applications and runs faster on a computer. Fig. 14 shows the curve shapes of the two different equations for Z_c, Z_o and the real and imaginary parts thereof.

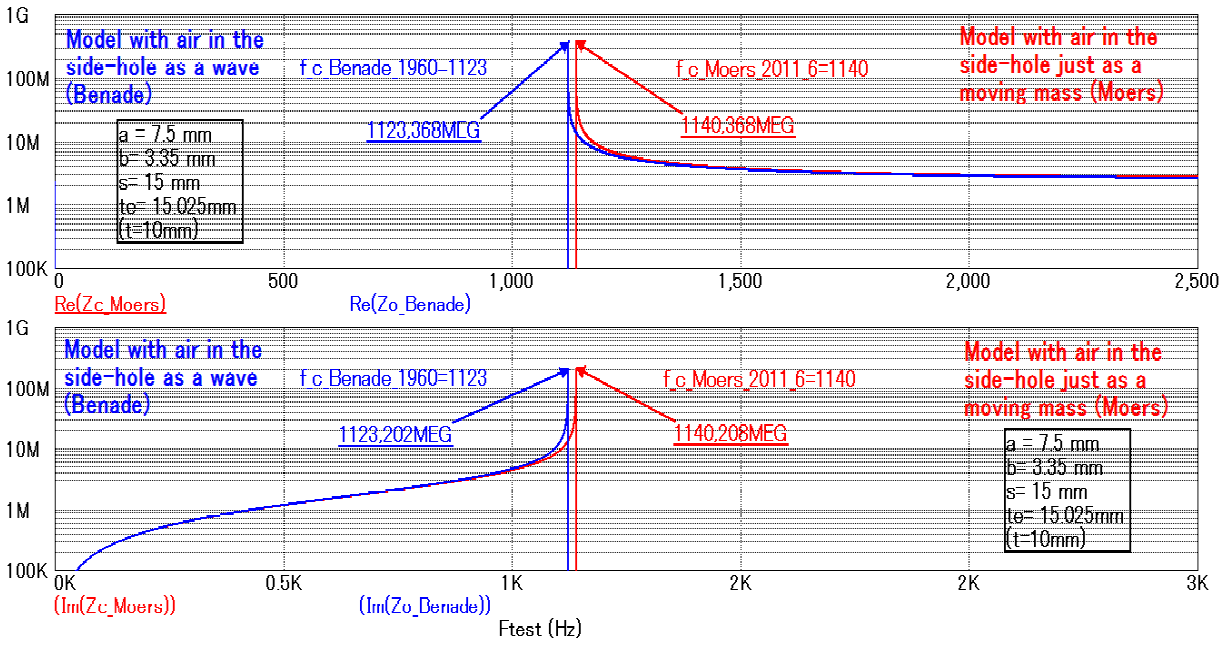

Fig. 14, comparison of f_c, side hole as a tube and only mass

7. APPENDIX 2

Here we describe the model (macro) for the lossy tube. There are two versions of the macro. One simple, for almost plane waves in tubes where Bessel functions are not needed. This is only valid for frequencies very much higher than fo=64*visc/(pi*rho*diam^2, cylindrical tube). The second model is also applicable for low frequencies (small diameters). It is based on Bessel functions and takes into account the friction on the walls of the tube. Simulation with the latter can be time consuming. The diameters used in the simulation (a_Benade = 15 mm, b_Benade = 3.35mm require only the simple model, so this is described here in detail.

The physical quantities used for the simulations are:

Standard temperature:	Celsius_standard = 23 °C
Speed of sound:	speed = 346.217 m/s
Standard pressure:	P_{atmos} = 101.325 Pa
Density of air (1% argon):	rho = 1.186 kg/m^3
Shear viscosity:	visc = 18.6*10^-6 kg/m/s
Dimensionless loss factor:	loss = 4.8
Specific heat ratio (c_p/c_v):	kappa = 1.40267
Prandtl number:	prandtl = 0.719551

The diameter of the cylindrical tube with circular cross section is “diam” and its length is named “length”. The frequency in Hz is called “F”. The circuit diagram of the macro is shown in Fig. 15. It includes the elements of the hybrid matrix shown in Fig. 16, together with the transmission matrix elements that are calculated from the propagation constant gamma and the characteristic impedance zwl1.

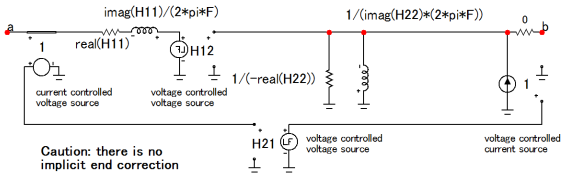

Fig. 15, circuit diagram of the lossy tube macro

Chain matrix lossy	
.define A11 (cosh(gamma*length))	.define A12 (zwl1*(sinh(gamma*length)))
.define A21 ((1/zwl1)*(sinh(gamma*length)))	.define A22 (cosh(gamma*length))
H matrix lossy	
.define H11 (A12/A22)	.define H12 (1/A22)
.define H21 (1/A22)	.define H22 (-A21/A22)

Fig. 16, Definition of the matrix elements

8. REFERENCES

[1] Benade, Arthur H.: On the mathematical theory of woodwind finger holes. J. Acoust. Soc. Am. 32 (1960) 1591–1608.

[2] Benade, Arthur H.: Fundamentals of Musical Acoustics. University Press, London, 1976. Reprinted and corrected in 1990 by Dover Publications, Mineola, N.Y.

[3] Micro Cap, Electronic Circuit Analysis Program, Spectrum Software, 1021 South Wolfe Road, Sunnyvale, CA 94086, programmed by Andy Thompson, Tim O'Brian, Bill Steele.

In Fig. 17 and Fig. 18 the definitions for gamma and zwl1 are shown in the form as they are used in the Circuit Analysis Program.

```
.define gamma

j*2*pi*F/speed*
(
   (1-2*j*(kappa-1)/
        (
           (-j*2*pi*F*rho*prandtl/
              (loss*visc)
           )^0.5*diam/2
        )
   )/
  (1+2*j/
     (
        (
           (-j*2*pi*F*rho/
              (loss*visc)
           )^0.5
        )*diam/2
     )
  )
)^0.5
```

Fig. 17, Definition of gamma

```
.define zwl1

rho*speed/(pi*(diam/2)^2)*
(1-2*j*(kappa-1)/
      (
         (-j*2*pi*F*rho*prandtl/
            (loss*visc)
         )^0.5
      )*diam/2
/
      (1+2*j/
         (
            (-j*2*pi*F*rho/
               (loss*visc)
            )^0.5
         )*diam/2
      )
)^0.5
```

Fig. 18, Definition of zwl1

[4] E. Moers, J. Kergomard: On the Cutoff Frequency of Clarinet-Like Instruments. Geometrical versus Acoustical Regularity, Acta Acustica united with Acustica, Vol. 97 (2011) 984 – 996

[5] Keefe, Douglas: Woodwind air column models, Journal of the Acoustical Society of America, 88 (1990), 35 -51

[6] Nederveen, C.J. et. al.: Corrections for Woodwind Tone-Hole Calculations, ACUSTICA - Acta Acustica Vol. 84 (1998) 957 – 966

[7] Dalmont, Jean-Pierre et al.: Experimental Determination of the Equivalent Circuit of an Open Side Hole: Linear and Non Linear Behaviour. Acta Acustica united with Acustica, Vol. 88 (2002) 567 – 575

[8] Noreland, Kergomard, Laloë, Vergez, Guillemain, Guilloteau: The Logical Clarinet: Numerical Optimization of the Geometry of Woodwind Instruments. Acta Acustica united with Acustica, Vol. 99 (2013) 615 – 628